Title

Identifying Heteroprotein Complexes in the Nuclear Envelope

Journal

Biophysical Journal, 118(1)

ISSN

0006-3495

Authors

Hennen, Jared

Hur, Kwang-Ho

Kohler, John

et al.

Publication Date

2020

DOI

10.1016/j.bpj.2019.11.020

Peer reviewed

Biophysical Journal
Article

Biophysical Society

Identifying Heteroprotein Complexes in the Nuclear Envelope

Jared Hennen,[1] Kwang-Ho Hur,[1] John Kohler,[1] Siddarth Reddy Karuka,[1] Isaac Angert,[1] G. W. Gant Luxton,[2] and Joachim D. Mueller[1,3,*]

[1]School of Physics and Astronomy, [2]Department of Genetics, Cell Biology, and Development, and [3]Department of Biomedical Engineering, University of Minnesota, Minneapolis, Minnesota

ABSTRACT The nucleus is delineated by the nuclear envelope (NE), which is a double membrane barrier composed of the inner and outer nuclear membranes as well as a ~40-nm wide lumen. In addition to its barrier function, the NE acts as a critical signaling node for a variety of cellular processes, which are mediated by protein complexes within this subcellular compartment. Although fluorescence fluctuation spectroscopy is a powerful tool for characterizing protein complexes in living cells, it was recently demonstrated that conventional fluorescence fluctuation spectroscopy methods are not suitable for applications in the NE because of the presence of slow nuclear membrane undulations. We previously addressed this challenge by developing time-shifted mean-segmented Q (tsMSQ) analysis and applied it to successfully characterize protein homo-oligomerization in the NE. However, many NE complexes, such as the linker of the nucleoskeleton and cytoskeleton complex, are formed by heterotypic interactions, which single-color tsMSQ is unable to characterize. Here, we describe the development of dual-color (DC) tsMSQ to analyze NE heteroprotein complexes built from proteins that carry two spectrally distinct fluorescent labels. Experiments performed on model systems demonstrate that DC tsMSQ properly identifies heteroprotein complexes and their stoichiometry in the NE by accounting for spectral cross talk and local volume fluctuations. Finally, we applied DC tsMSQ to study the assembly of the linker of the nucleoskeleton and cytoskeleton complex, a heteroprotein complex composed of Klarsicht/ANC-1/SYNE homology and Sad1/UNC-84 (SUN) proteins, in the NE of living cells. Using DC tsMSQ, we demonstrate the ability of the SUN protein SUN2 and the Klarsicht/ANC-1/SYNE homology protein nesprin-2 to form a heterocomplex in vivo. Our results are consistent with previously published in vitro studies and demonstrate the utility of the DC tsMSQ technique for characterizing NE heteroprotein complexes.

SIGNIFICANCE Protein complexes found within the nuclear envelope (NE) play a vital role in regulating cellular functions ranging from gene expression to cellular movement. However, the assembly state of these complexes within their native environment remains poorly understood, which is compounded by a general lack of fluorescence techniques suitable for quantifying the oligomeric state of NE protein complexes. This study aims at addressing this issue by introducing dual-color time-shifted mean-segmented Q analysis as a fluorescence fluctuation method specifically designed to identify the average oligomeric state of heteroprotein complexes within the NE of living cells.

INTRODUCTION

Fluorescence fluctuation spectroscopy (FFS) refers to a collection of related biophysical techniques that exploit the stochastic intensity of fluorescently labeled biomolecules passing through a small observation volume created by confocal or two-photon microscopy (1). The primary parameters accessible by FFS are the concentration, mobility, and oligomeric state of the labeled biomolecule (1). Although the original analysis of FFS results was based on the autocorrelation function (ACF), many other methods have been introduced over the years, each with its own strengths and weaknesses (2–5). An important advance in FFS was the introduction of dual-color (DC) FFS for identifying interactions between two species of biomolecules labeled with spectrally distinct fluorophores (6). In DC FFS, the emission of the fluorophores is separated by color into two detection channels. Heterotypic interactions between the two species lead to synchronized temporal

Submitted July 19, 2019, and accepted for publication November 18, 2019.

*Correspondence: mueller@physics.umn.edu

Jared Hennen and Kwang-Ho Hur contributed equally to this work.

Editor: Jason Swedlow.

https://doi.org/10.1016/j.bpj.2019.11.020

fluctuations in both channels, which are recognized by the cross correlation function (CCF) of the two detected signals. In addition to CCF, other analysis techniques have been introduced for quantifying heterospecies interactions from FFS experiments (7,8).

Because FFS is an equilibrium technique that passively observes fluctuations, it is well suited for applications in live cells (9). Cellular proteins can be conveniently labeled by genetic tagging with one of the many available fluorescent proteins (10). Brightness, which characterizes the intrinsic fluorescence intensity of a molecule, is an important FFS parameter because it contains information about the stoichiometry of fluorescently tagged protein complexes (11). For example, the brightness of monomeric proteins tagged with EGFP will increase upon their association into homo-oligomers as each protein complex contains several fluorescent labels. This concept has been generalized to include differently colored fluorophores to characterize heteroprotein complexes (7). Although FFS brightness analysis has been successfully used to quantify protein-protein interactions within the cytoplasm, nucleoplasm, and at the plasma membrane (9,12,13), its extension to the nuclear envelope (NE) has proven challenging (14).

The NE consists of an inner nuclear membrane (INM) and outer nuclear membrane (ONM) separated by a ~40-nm-thick fluid layer, known as the lumen or perinuclear space. Although the NE has been identified as a critical signaling node of the cell (15), a mechanistic understanding of how these heteroprotein complexes assemble remains limited because of the lack of quantitative biophysical techniques suitable for use in the NE. To address this challenge, we explored the use of single-color (SC) FFS for characterizing homoprotein association in the NE of living cells (14,16). We found that slow undulations of the nuclear membranes give rise to local volume fluctuations that are not properly accounted for by conventional FFS methods (14). We overcame this obstacle by introducing mean-segmented Q (MSQ) analysis as well as time-shifted MSQ (tsMSQ), a significantly improved version of MSQ (14,17,18). We demonstrated that these techniques successfully identify the mobility and homo-oligomeric state of NE proteins (14).

This study extends FFS analysis of heteroprotein complexes to the NE by introducing DC tsMSQ, a generalized form of regular tsMSQ. The DC tsMSQ framework includes heterospecies partitioning (HSP) (7) and effectively eliminates complications due to spectral cross talk in the characterization of heterotypic protein interactions as verified by control experiments. Our study demonstrates that local volume fluctuations of the NE are a significant challenge for conventional DC FFS analysis, which prompted the development of DC tsMSQ. We first verified the foundation of DC tsMSQ using pairs of interacting and noninteracting proteins measured in the cytoplasm and in the NE. In addition, control experiments using both luminal and nuclear membrane-associated proteins were conducted to illustrate the influence of the nuclear membrane undulations on DC tsMSQ analysis.

To demonstrate the power of DC tsMSQ, we applied it toward studying the assembly of the linker of nucleoskeleton and cytoskeleton (LINC) complex in the NE of living cells. This NE-spanning molecular bridge mediates mechanical force transmission into the nucleoplasm and is required for several fundamental cellular processes, including cell division, DNA damage repair, meiotic chromosome pairing, mechanoregulation of gene expression, and nuclear positioning (19). The LINC complex is formed by a direct transluminal heterotypic interaction between the cytoskeletal-binding ONM *Klarsicht/ANC-1/SYNE* homology (KASH) proteins and the nuclear lamina-binding INM *Sad1/UNC-84* (SUN) proteins (20). Previous in vitro biochemical and structural studies revealed that the luminal domain of SUN2 homotrimerizes and that the luminal domain of the KASH protein nesprin-2 binds in the grooves formed at the interface of two adjacent interacting SUN2 monomers (21,22). Thus, the homotrimerization of the SUN2 luminal domain enables the recruitment of 3 nesprin-2 luminal domains, resulting in the assembly of a SUN2-nesprin-2 heterohexamer. We recently succeeded in directly measuring the homotrimerization of the EGFP-tagged luminal domain of SUN2 in the NE of living cells by SC FFS (16). Here, we utilize DC tsMSQ to directly observe the heterotypic interactions formed between the EGFP-tagged SUN2 luminal domain and an mCherry-tagged construct that encodes the last three spectrin-like repeats (SRs), the transmembrane domain, and the luminal KASH peptide of nesprin-2 in the NE. This work establishes the theoretical and practical framework necessary for future quantitative studies of LINC complex assembly within the NE of living cells as well as the characterization of additional heterotypic interactions between proteins within this relatively unexplored subcellular environment.

MATERIALS AND METHODS

Experimental setup

Brightness measurements were performed as previously described (7,9). Briefly, FFS data were acquired on a custom built two-photon microscope with a 63× C-Apochromat water-immersion objective with numerical aperture (NA) = 1.2 (ZEISS, Oberkochen, Germany) using an excitation wavelength of 1000 nm and an average power after the objective in the range of 0.3–0.4 mW. A dichroic mirror centered at 580 nm (FF580-FDi01; Semrock, Rochester, NY) was used to split the emission path into two channels. An additional 84-nm wide bandpass filter centered at 510 nm (FF01-510/84; Semrock) was placed before the green channel to remove any reflected fluorescence from mCherry. Photon counts were detected using avalanche photodiodes (SPCM-AQ-141 APD; PerkinElmer, Waltham, MA), recorded with a Flex04-12D card (Correlator.com, Bridgewater, NJ) sampled at 20 kHz and analyzed using programs written in IDL (Interactive Data Language) 8.7 (Research Systems, Boulder, CO). Z-scans were performed using an arbitrary waveform generator (model number 33522A; Agilent Technologies, Santa Clara, CA) to move a PZ2000 piezo stage (Applied Scientific Instrumentation, Eugene, OR) axially. The waveform created by the generator was

a linear ramp function with a peak-to-peak amplitude of 1.6 V, corresponding to 24.1 μm of axial travel and a period of 10 s for a speed of 4.82 μm/s.

Measurement procedure

EGFP (G) calibration measurements were performed in the cytoplasm of EGFP-expressing U2OS cells, as previously described (9,12), to obtain its brightness in both the green and red channels ($\lambda_{g,G}$ and $\lambda_{r,G}$, respectively). Additional calibration measurements were performed in the cytoplasm of U2OS cells expressing EGFP-RARLBD-mCherry (7) to obtain the brightness $\lambda_{r,Ch}$ of mCherry (Ch) in the red channel, which accounts for the previously described two-state brightness of this fluorescent protein (7). These calibration values were then converted to Q values for the NE using $Q = \gamma_2 \lambda T_s$, where γ_2 is the shape factor for a two-dimensional Gaussian point spread function, and T_s is the sampling time (12,23). Measurements in the NE were performed as previously described (14,24) by first using epifluorescence to identify cells expressing the relevant constructs. FFS data were then acquired by taking z-scans through the nucleus, which were analyzed as previously described (14,25). Next, the two-photon beam was focused on the ventral NE followed by the dorsal NE and ~60 s of intensity fluctuation data were obtained at each location. These data were analyzed as described in Theory to obtain the normalized HSP brightness vector $\mathbf{b} = (b_g, b_r)$ (7,26). The normalized brightness values were corrected for two-state brightness and fluorescence resonance energy transfer as previously described (7,27). The average number of molecules in the observation volume was determined by $N_g = \langle F_g \rangle / \lambda_{g,G}$ and $N_r = (\langle F_r \rangle - f_{ct} \times \langle F_g \rangle) / \lambda_{r,Ch}$, where $\langle F_i \rangle = \langle k_i \rangle / T_S$ and f_{ct} is the spectral cross talk of EGFP given by $Q_{r,G}/Q_{g,G}$ (7). We limited our measurements to expression levels of $N \geq 10$, which, for our experiments, corresponds to a minimum signal to background ratio of 10:1. These conditions ensure that the influence of background on the recovered FFS parameters is negligible.

Sample preparation

Experiments were conducted using transiently transfected U2OS cells (ATCC, Manassas, VA) maintained in DMEM with 10% fetal bovine serum (HyClone Laboratories, Logan, UT). U2OS cells were subcultured into 24-well glass-bottom plates (Cellvis, Sunnyvale, CA) before transfection. GenJet (SignaGen Laboratories, Rockville, MD) was used to transiently transfect cells 12–24 h before measurement, according to the instructions of the manufacturer. The growth medium was replaced with Dulbecco's phosphate-buffered saline containing calcium and magnesium (BioWhittaker, Walkerville, MD) immediately before measuring.

Reagents

Restriction enzymes were either purchased from New England BioLabs (Ipswich, MA) or Promega (Madison, WI). Calf Intestinal Phosphatase, Phusion DNA polymerase, T4 DNA ligase, and T4 polynucleotide kinase were also purchased from New England BioLabs. All other chemicals were purchased from Sigma-Aldrich (St. Louis, MO) unless otherwise specified. The Wizard SV Gel and PCR Clean-Up System were purchased from Promega, whereas the GeneJet Plasmid Midiprep Kit was purchased from Thermo Fisher Scientific (Waltham, MA).

DNA constructs

The generation of SS-EGFP, SS-EGFP-torsinA$^{\text{NTD-2xLeu}}$, SS-EGFP-SUN2$^{595–731}$, and SS-EGFP-SUN2$^{261–731}$ constructs were described previously (14,16). The generation of SS-mCherry-KDEL, the SUN domain-linked SS-EGFP-SUN2$^{595–731}$-mCherry (SS-EGFP-SL-mCherry), and mCherry-SR-KASH2 constructs are described in Supporting Materials and Methods, Section 6.

Theory

Dual-channel tsMSQ$_{\sigma\rho}$

The single channel tsMSQ was generalized to dual-channel tsMSQ$_{\sigma\rho}$ (Supporting Materials and Methods, Section 1) with the subscripts σ and ρ specifying the detection channel. A single diffusing species is described by the following:

$$\text{tsMSQ}_{\sigma\rho,D}(T; Q_\rho, \tau_D) = Q_\rho \text{tsF}_D(T; \tau_D), \tag{1}$$

whereas the exponential correlation process caused by the local volume fluctuations of the NE is given by the following:

$$\text{tsMSQ}_{\sigma\rho,E}(T; A_\rho, \tau_0) = A_\rho \text{tsF}_E(T; \tau_0), \tag{2}$$

as derived in Supporting Materials and Methods, Section 2. A sample consisting of a single diffusing species in the lumen of the NE experiences local volume fluctuations and is described by the addition of Eqs. 1 and 2 (14), as follows:

$$\text{tsMSQ}_{\sigma\rho,\text{DE}}(T) = Q_\rho \text{tsF}_D(T; \tau_D) + A_\rho \text{tsF}_E(T; \tau_0). \tag{3}$$

The time-shifted correlation functions tsF_D and tsF_E are defined in terms of second-order binning functions $\text{B}_{2,\text{D}}(T)$ and $\text{B}_{2,\text{E}}(T)$ (4,14,18,28). Explicit formulas are found in Supporting Materials and Methods, Section 3. Because Eqs. 1 and 2 must reproduce the single channel case for $\sigma = \rho$, the amplitudes Q_ρ and A_ρ are given by $Q_\rho = \gamma_2 \lambda_\rho T_s$ and $A_\rho = c^2 \lambda_\rho T_s N$, respectively (14,18). The brightness of the fluorescent molecule in the ρ channel is λ_ρ, the number of molecules in the observation volume is N, and the shape factor of the observation volume is γ_2. The factor c is determined by the fluctuations in the gap distance h separating the INM and ONM, $c = \sqrt{\langle \delta h^2 \rangle} / \langle h \rangle$ (14). The diffusion time and the characteristic time of the volume fluctuations are given by τ_D and τ_0, respectively.

The two detection channels used for DC FFS are labeled as green (g) and red (r). We define the DC tsMSQ function as follows:

$$\text{tsMSQ}(T) = \begin{bmatrix} \text{tsMSQ}_{\text{gg}}(T) \\ \text{tsMSQ}_{\text{gr}}(T) \end{bmatrix}. \tag{4}$$

We refer to tsMSQ_{gg} as the autocorrelation tsMSQ of the green detection channel and tsMSQ_{gr} as the cross correlation tsMSQ of the green and red channel. Thus, DC tsMSQ of a diffusing species is described by the following:

$$\text{tsMSQ}_\mathbf{D}(T) = \mathbf{Q}\ \text{tsF}_D(T; \tau_D), \tag{5}$$

and in the presence of volume fluctuations, the exponential correlation process,

$$\text{tsMSQ}_\mathbf{E}(T) = \mathbf{A}\ \text{tsF}_E(T, \tau_0), \tag{6}$$

is added, resulting in the following:

$$\text{tsMSQ}_\mathbf{DE}(T) = \text{tsMSQ}_\mathbf{D}(T) + \text{tsMSQ}_\mathbf{E}(T). \tag{7}$$

DC tsMSQ reduces to the same functional form as SC tsMSQ but with vector amplitudes $\mathbf{Q} = (Q_g, Q_r)$ and $\mathbf{A} = (A_g, A_r)$, which are scaled by tsF_D and tsF_E, respectively. Finally, for a fit to a model with S diffusing species, the $\mathbf{tsMSQ_D}$ term is replaced by the following:

$$\text{tsMSQ}_\mathbf{D}(T) = \sum_{i=1}^{S} f_i \mathbf{Q}_i \text{tsF}_D(T; \tau_{D,i}), \tag{8}$$

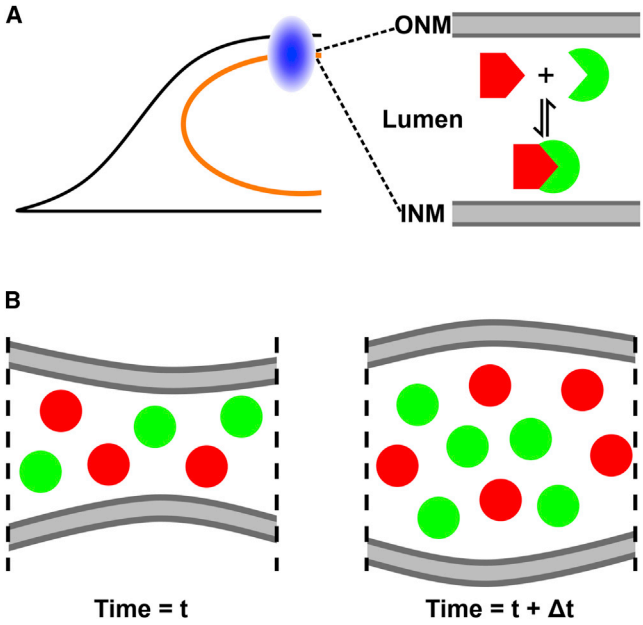

FIGURE 1 FFS at the NE. (*A*) Shown is an illustration of a cell expressing potentially interacting green and red fluorescently labeled NE proteins with the two-photon excitation volume (*blue oval*) focused at its NE (*orange circle*), which consists of the INM and ONM separated by a ~40-nm-thick lumen. (*B*) Shown is an illustration of the time-dependent local volume fluctuations caused by nuclear membrane undulations, which give rise to coupled intensity variations of the noninteracting green and red fluorescently labeled proteins. To see this figure in color, go online.

where $\mathbf{Q}_i$ and $\tau_{D,i}$ are the Q-vector and diffusion time of the i^{th} species, respectively. The fractional intensity f_i of the i^{th} species is defined by the ratio of the green-channel intensity of the i^{th} species to the total intensity $\langle F_g \rangle = \sum_{j=1}^{S} \langle F_{g,j} \rangle$ of the green channel, $f_i = \langle F_{g,i} \rangle / \langle F_g \rangle$, as described in the Supporting Materials and Methods. The total Q-vector, $\overline{\mathbf{Q}}$, of the sample is defined by the following:

$$\overline{\mathbf{Q}} = \sum_{i=1}^{S} f_i \mathbf{Q}_i, \tag{9}$$

and represents the ensemble average over all species.

DC tsMSQ and HSP

We previously demonstrated that the complications in interpreting the results of FFS experiments in the presence of spectral cross talk are avoided by HSP analysis (7). HSP requires that there is no spectral leakage of the red-emitting mCherry into the green emission channel, which is accomplished by choosing the appropriate filters (7). Thus, the two fluorescent proteins EGFP (G) and mCherry (Ch) are characterized by their respective Q-vectors $\mathbf{Q}_G = (Q_{g,G}, Q_{r,G})$ and $\mathbf{Q}_{ch} = (0, Q_{r,Ch})$. The Q-vector (Eq. 9) determined by DC tsMSQ analysis may be expressed as a linear combination of the Q-vectors of EGFP and mCherry, as follows:

$$\overline{\mathbf{Q}} = b_g \mathbf{Q}_G + b_r \mathbf{Q}_{Ch}, \tag{10}$$

where the coefficients b_g and b_r represent the normalized brightness associated with the corresponding fluorescent proteins (7,29). The tuple (b_g, b_r) characterizes the brightness vector of the heterospecies present in the sample. The heterospecies comprises all EGFP-labeled proteins and heteroprotein complexes carrying both EGFP and mCherry. Monomeric or oligomeric complexes that only contain the mCherry label are partitioned out by HSP. For example, a noninteracting monomeric EGFP-labeled species is described by an HSP brightness vector of (1, 0), whereas a heterodimer containing one EGFP and one mCherry label are described by an HSP brightness vector of (1, 1). An HSP brightness vector of (1, y) describes an EGFP-labeled protein that on average is associated with y mCherry-labeled proteins (7). A graphical representation of these examples is provided in Fig. S1. The HSP brightness vector (b_g, b_r) is affected by fluorescent labels with dark states and multiple brightness states as well as by fluorescence resonance energy transfer, which bias the interpretation (7,27). These effects were accounted and corrected for as previously described (7,27). A derivation of HSP for DC tsMSQ is found in Supporting Materials and Methods, Section 5.

RESULTS

Initial experiments were performed on a noninteracting pair of proteins located in the lumen of the NE (Fig. 1 *A*). Specifically, we used SS-EGFP and SS-mCherry-KDEL, which have been found to be monomeric proteins within the NE by SC FFS (Fig. S2; (14)). EGFP and mCherry were chosen as labels because this pair has been characterized extensively by DC FFS and have a wide separation in their emission color (7,10). The signal sequence (SS) of the luminal ATPase torsinA, which is cleaved after protein expression, ensures the presence of EGFP in the lumen of the NE (30). The C-terminus of SS-mCherry was additionally fused to the endoplasmic reticulum retention signal KDEL to ensure its efficient targeting to the lumen. DC FFS data were collected at the NE of U2OS cells co-expressing SS-EGFP and SS-mCherry-KDEL. The ACFs of the fluorescence collected by the green and red detection channels were calculated (G_{gg} and G_{rr}, respectively) as well as the CCF G_{gr} of both channels. We observed a positive CCF amplitude (Fig. 2), which was not unexpected for a noninteracting pair of fluorescent proteins because spectral cross talk leads to a positive CCF component (31). This cross talk-induced CCF function is predicted by (31) the following:

$$\mathrm{CCF}_{\mathrm{ct}}(\tau) = G_g(\tau) f_{\mathrm{ct}} \frac{\langle F_g \rangle}{\langle F_r \rangle}, \tag{11}$$

with $\langle F_g \rangle$ and $\langle F_r \rangle$ representing the mean fluorescence intensities of the green and red channel, respectively. The cross talk in our setup is caused by the detection of the long wavelength emission of EGFP in the red detection channel (32), which is characterized by the cross talk intensity fraction f_{ct}. The observed CCF has to significantly exceed this baseline for a positive identification of heterotypic protein interactions (31). The computed $\mathrm{CCF}_{\mathrm{ct}}$ (τ) (*solid blue lines*, Fig. 2) is not significantly different from the observed CCF for the data taken at low expression levels (Fig. 2 *A*) but is significantly below the experimental CCF at medium (Fig. 2 *B*) and high expression levels (Fig. 2 *C*). This observation is counterintuitive as it suggests the onset of interactions between EGFP and mCherry-KDEL at higher concentrations. We further noticed a significant change in the shape of the ACF of both channels as well

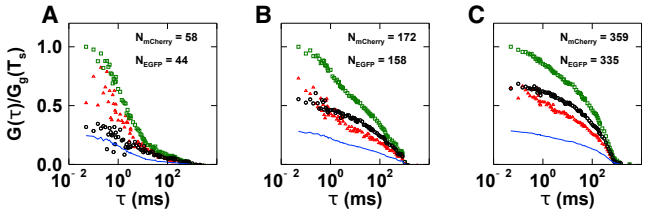

FIGURE 2 ACF and CCF analysis of DC FFS data collected in the NE of cells expressing SS-EGFP and SS-mCherry-KDEL at low (*A*), medium (*B*), and high (*C*) levels of protein expression. The number of proteins in the observation volume is given by N_{EGFP} and $N_{mCherry}$. The red and green channel ACFs are shown with red triangles and green squares, respectively. The CCF is graphed as black circles, and the calculated CCF from spectral cross talk (CCF_{ct}) is shown by the blue line. All correlation curves are divided by the amplitude of the ACF of the green channel, $G_{gg}(T_s)$, with a lag time equal to the sampling time T_s. To see this figure in color, go online.

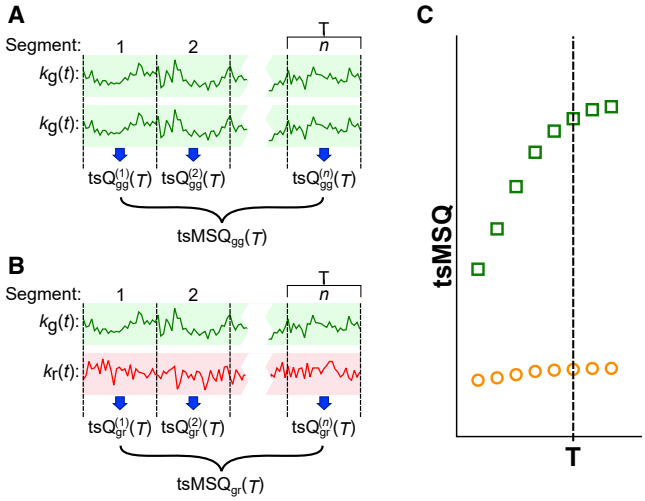

FIGURE 3 Conceptual illustration of the DC tsMSQ algorithm. (*A*) The fluorescence intensity trace of the green channel, k_g, is divided into n segments of period T. The time-shifted Q value of segment i, $tsQ_{gg}^{(i)}(T)$, is calculated from k_g and a copy of k_g, according to Eq. S3. Averaging over the time-shifted Q values determines the $tsMSQ_{gg}$ for segment time T. (*B*) The algorithm for calculating the cross correlation $tsMSQ_{gr}$ follows the same procedure as described in (*A*) but replaces the copy of k_g with the intensity of the red channel, k_r. (*C*) The autocorrelation $tsMSQ_{gg}$ (*green squares*) and cross correlation $tsMSQ_{gr}$ (*orange circles*) are constructed by repeating the procedures shown in (*A* and *B*) for a range of segment times T. To see this figure in color, go online.

as the CCF with increasing concentration (Fig. 2), which was unexpected because the diffusion process is independent of concentration. These changes in the ACF are specific to the NE environment (14) and are not observed in the cytoplasm as confirmed by a control experiment performed in the cytoplasm of cells expressing EGFP and mCherry. Specifically, measurements performed in these cells showed a concentration-independent shape of the ACF as well as a strong overlap between the computed CCF_{ct} (τ) and the CCF over a wide range of expression levels (Fig. S3), indicating the absence of significant interactions between EGFP and mCherry within the cytoplasm.

The unusual behavior of the experimental ACF of FFS data collected within the NE was traced to undulations of the nuclear membranes (14). These membrane undulations introduce local volume fluctuations that modulate the fluorescence intensity signals received from SS-EGFP and SS-mCherry-KDEL (Fig. 1 *B*). This additional fluctuation process not only affects the ACF but also the CCF as the volume fluctuations lead to concomitant intensity variations in both the green and red channels. We previously demonstrated that the slow membrane undulations lead to biases in ACF analysis (14). To overcome this challenge, we replaced ACF with MSQ analysis and, more recently, with the improved tsMSQ algorithm (14,18). Both methods have proven to be robust for measuring homotypic protein interactions within the NE of living cells (16,24). To extend cross correlation analysis to DC FFS data obtained in the NE, we generalize SC to DC tsMSQ. Two subscripts are added to distinguish the different tsMSQ functions. The SC tsMSQ from the green channel is identified by $tsMSQ_{gg}$, whereas the cross correlation tsMSQ between the green and the red channel is described by $tsMSQ_{gr}$ (Fig. 3). The autocorrelation $tsMSQ_{gg}$ is calculated from the fluorescence intensity of a single channel using the standard tsMSQ algorithm (Fig. 3 *A*). The cross correlation $tsMSQ_{gr}$ follows the same procedure but utilizes the intensity traces of both channels (Fig. 3 *B*).

We reanalyzed the FFS data of SS-EGFP and SS-mCherry-KDEL taken in the NE (Fig. 2) using the experimental $tsMSQ_{gg}$ (green squares) and $tsMSQ_{gr}$ (red circles) curves (Figs. 4 *A* and S4, *A* and *B*). For two noninteracting proteins undergoing simple diffusion in the lumen, the cross correlation $tsMSQ_{gr}$ should be entirely determined by the cross talk f_{ct} from EGFP into the red channel and the membrane undulations of the NE, which contribute a correlation amplitude proportional to the average intensity (14). Thus, the $tsMSQ_{gr}$ curve for two noninteracting luminal proteins is predicted to be the following

$$tsMSQ_{gr}^{(-)}(T) = f_{ct}tsMSQ_{gg,D}(T;\tau_D,Q_g) + \frac{\langle F_r\rangle}{\langle F_g\rangle}tsMSQ_{gg,E}(T;\tau_0,A_g), \quad (12)$$

where $tsMSQ_{gg,D}(T, \tau_D, Q_g)$ and $tsMSQ_{gg,E}(T, \tau_0, A_g)$ are model functions (Eqs. 1 and 2) that describe the diffusion and exponential components of $tsMSQ_{gg}$, respectively, whereas $\langle F_i\rangle$ represents the mean intensity in the i^{th} channel. The green-channel $tsMSQ_{gg}$ was fit to a single species diffusion model with an exponential correlation term (Eq. 3) to account for nuclear membrane undulations, enabling the calculation of the predicted cross correlation $tsMSQ_{gr}^{(-)}$ in the absence of interactions from Eq. 12 (*blue line*, Figs. 4 *A* and S4, *A* and *B*). The predicted $tsMSQ_{gr}^{(-)}$ and the experimental $tsMSQ_{gr}$ closely overlap, demonstrating the absence

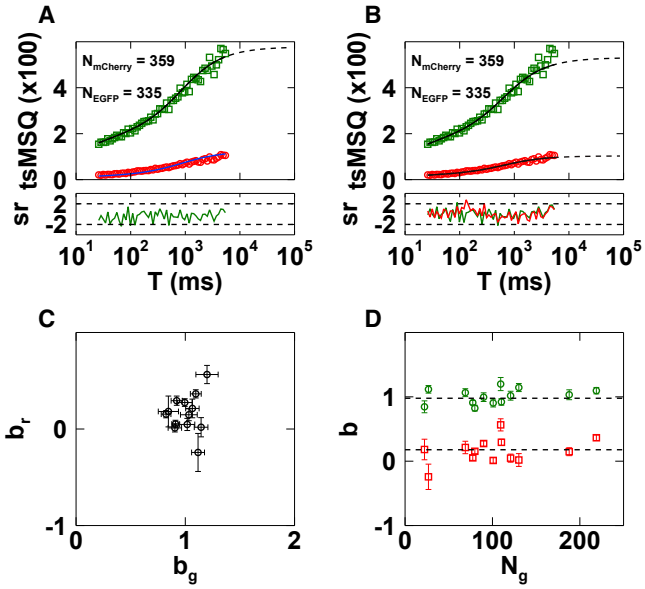

FIGURE 4 DC tsMSQ analysis of measurements performed in the NE of cells ($n = 16$) co-expressing SS-EGFP and SS-mCherry-KDEL. (*A*) Shown are tsMSQ curves (*symbols*) with predicted $\text{tsMSQ}_{\text{gr}}^{(-)}$ curve (*blue line*) derived from a fit to tsMSQ_{gg} (*black line*) and standard residuals (sr). The tsMSQ_{gg} and tsMSQ_{gr} curves are shown with green squares and red circles, respectively. (*B*) Shown are tsMSQ curves (*symbols*) with fit to Eq. 7 (*black*). (*C*) Shown is b_r versus b_g with standard deviations (error bars). (*D*) Shown are b_g (*green circles*) and b_r (*red squares*), with respective standard deviations (error bars), versus N_g with means (*dashed lines*) and SDs of $b_g = 1.0 \pm 0.2$ and $b_r = 0.16 \pm 0.13$. To see this figure in color, go online.

of protein interactions between luminal EGFP and mCherry-KDEL. These results demonstrate that tsMSQ_{gg} accurately predicts the cross correlation $\text{tsMSQ}_{\text{gr}}^{(-)}$ curve of a noninteracting pair of proteins within the NE.

This initial validation of the theory prompted us to analyze FFS data with DC tsMSQ, which simultaneously describes the green-channel autocorrelation and the cross correlation tsMSQ (Eq. 4), $\mathbf{tsMSQ} = [\text{tsMSQ}_{\text{gg}}, \text{tsMSQ}_{\text{gr}}]$. We fit both tsMSQ curves to Eq. 7, which describes a single diffusion species in the presence of volume fluctuations. The fit and data are in very good agreement (Figs. 4 *B* and S4, *C* and *D*) with reduced chi-squared values close to one. From these fits, we obtained the mean fit parameters and their uncertainties, which were derived from the covariance matrix. The analysis was performed on $n = 16$ cells to collect fit parameters and uncertainties over a range of expression values. The amplitude $\mathbf{A} = (A_g, A_r)$ is expected to increase linearly with the fluorescence intensity, which agrees with the data (Fig. S5 *A*). The characteristic time of the volume fluctuations is independent of the concentration with a mean time of 0.3 s, closely mirroring results obtained in previous work (Fig. S6 *A*; (14)).

The fitted Q-vector $\overline{\mathbf{Q}} = (\overline{Q}_g, \overline{Q}_r)$ was converted into the normalized brightness $\mathbf{b} = (b_g, b_r)$ (Fig. 4 *C*), as described in Theory. The values of the brightness plot scatter around $\mathbf{b} = (1, 0)$, which is consistent for the SS-EGFP species containing one EGFP label and zero mCherry labels. These **b** values showed no dependence on the concentration of SS-EGFP (Fig. 4 *D*). As discussed in Theory, DC tsMSQ was designed to identify HSP parameters. Thus, any purely red-emitting species is filtered out by HSP. As a consequence, we expected the noninteracting SS-mCherry-KDEL species to be invisible to the analysis, which is confirmed by the brightness plot. Consequently, the recovered diffusion times apply to the SS-EGFP species (Fig. S7 *A*). Their values are concentration independent with a mean value of 1.7 ms, which is consistent with previous results (14,18).

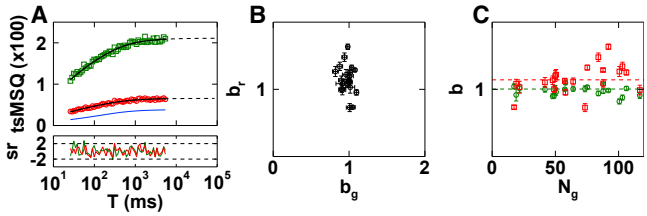

FIGURE 5 DC tsMSQ analysis of measurements obtained in the NE of cells ($n = 24$) expressing SS-EGFP-SL-mCherry. (*A*) Shown are tsMSQ curves (*symbols*) with fits (*black lines*), standard residuals (sr), and predicted $\text{tsMSQ}_{\text{gr}}^{(-)}$ curve (*blue line*). The tsMSQ_{gg} and tsMSQ_{gr} curves are shown with green squares and red circles, respectively. (*B*) Shown is b_r versus b_g with standard deviations (error bars). (*C*) Shown are b_g (*green circles*) and b_r (*red squares*), with respective standard deviations (error bars), versus N_g with means (*dashed lines*) and SDs of $b_g = 0.96 \pm 0.06$ and $b_r = 1.1 \pm 0.3$. To see this figure in color, go online.

As an additional control, we reanalyzed the cytoplasmic EGFP and mCherry data (Fig. S3) using DC tsMSQ with a fit to a single diffusing species (Eq. 5). The data and fit closely match (Fig. S8, *A–C*), with the recovered HSP brightness values $\mathbf{b} = (b_g, b_r)$ centered near (1, 0) in a brightness plot, which is consistent with the EGFP species (Fig. S8, *D* and *E*). The fitted diffusion time is concentration independent with a mean value of 0.8 ms (Fig. S7 *B*), which agrees with previously published experiments (33).

After establishing that DC tsMSQ properly identifies noninteracting proteins within the NE and the cytoplasm, we next examined the tandem heterodimer SS-EGFP-SL-mCherry. This construct carries both EGFP and mCherry separated by a linker (SL) and mimics a strongly interacting pair of proteins forming a heterodimeric complex. As expected, DC FFS measurements of SS-EGFP-SL-mCherry in the NE produced a cross correlation tsMSQ_{gr} curve that significantly exceeded the predicted baseline $\text{tsMSQ}_{\text{gr}}^{(-)}$ for noninteracting proteins (Fig. 5 *A*). The DC tsMSQ curves were readily modeled by a fit to Eq. 7 (Fig. 5 *A*) with reduced chi-squared values of 1.06. The HSP brightness values were centered around (1, 1), reflecting the presence of complexes with an average composition of one EGFP and one mCherry label as expected for the heterodimer (Fig. 5 *B*). The diffusion time of the heterodimer identified by fitting is concentration independent (Fig. S7 *C*). The **A** and τ_0 values obtained for the volume fluctuations agree with the expected behavior (Figs. S5 *B* and S6 *B*). These results demonstrate that DC tsMSQ

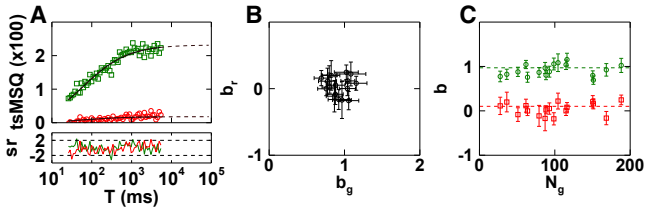

FIGURE 6 DC tsMSQ analysis of measurements performed in the NE of cells ($n = 20$) co-expressing SS-EGFP-torsinA$^{NTD\text{-}2xLeu}$ and SS-mCherry-KDEL. (*A*) Shown are tsMSQ curves (*symbols*) with fits (*black lines*) and standard residuals (sr). The tsMSQ$_{gg}$ and tsMSQ$_{gr}$ curves are shown with green squares and red circles, respectively. (*B*) Shown is b_r versus b_g with standard deviations (error bars). (*C*) Shown are b_g (*green circles*) and b_r (*red squares*), with respective standard deviations (error bars), versus N_g with means (*dashed lines*) and SDs of $b_g = 0.97 \pm 0.18$ and $b_r = 0.08 \pm 0.12$. To see this figure in color, go online.

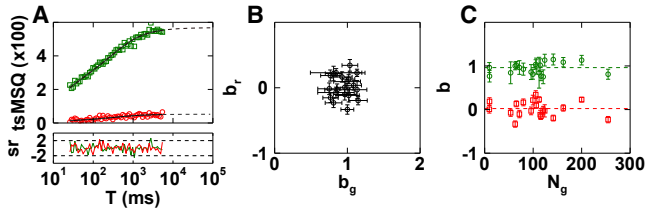

FIGURE 7 DC tsMSQ analysis of measurements performed in the NE of cells ($n = 20$) co-expressing SS-EGFP-SUN2$^{595–731}$ and mCherry-SR-KASH2. (*A*) Shown are tsMSQ curves (*symbols*) with fits (*black lines*) and standard residuals (sr). The tsMSQ$_{gg}$ and tsMSQ$_{gr}$ curves are shown with green squares and red circles, respectively. (*B*) Shown is b_r versus b_g with standard deviations (error bars). (*C*) Shown are b_g (*green circles*) and b_r (*red squares*), with respective standard deviations (error bars), versus N_g with means (*dashed lines*) and SDs of $b_g = 0.96 \pm 0.13$ and $b_r = 0.0 \pm 0.2$. To see this figure in color, go online.

can be used to accurately identify the presence of heterodimeric protein complexes in the NE of living cells.

Although the fluorescence intensity of luminal proteins is affected by volume fluctuations in the NE (Fig. 1 *B*), the fluorescence intensity of membrane-associated proteins is not affected by these volume fluctuations as demonstrated in previous work using SC FFS (14). To test this difference between luminal and membrane-bound proteins in the context of DC tsMSQ, we performed DC FFS experiments in the NE of cells expressing the membrane-bound SS-EGFP-torsinA$^{NTD\text{-}2xLeu}$ and the luminal SS-mCherry-KDEL. Because torsinA$^{NTD\text{-}2xLeu}$ is a transmembrane domain (34), its presence ensures that EGFP is anchored to the nuclear membrane.

Although the fluorescence signal generated by the luminal SS-mCherry-KDEL includes volume fluctuations, the fluorescence signal generated from the membrane-bound SS-EGFP-torsinA$^{NTD\text{-}2xLeu}$ does not. Because DC tsMSQ filters out any purely red fluorescing species, the data are expected to only contain the membrane-bound green fluorescing species. Consequently, we fit the DC tsMSQ curves to a model containing only a diffusing species and no exponential process (Eq. 5), which agreed well with the data ($\chi^2_\nu = 1.07$). The fit recovered HSP brightness values **b** that are clustered around (1, 0) (Fig. 6 *B*) and show no concentration dependence (Fig. 6 *C*), which is consistent with SS-EGFP-torsinA$^{NTD\text{-}2xLeu}$ being monomeric. The diffusion times for SS-EGFP-torsinA$^{NTD\text{-}2xLeu}$ (Fig. S7 *D*) have a mean and SD of 16 ± 4 ms, which is in agreement with previously published results for this construct (14).

We next used DC tsMSQ to study the assembly of LINC complexes composed of SUN2 and nesprin-2 in vivo by investigating the ability of the SUN2 luminal domain to form a heterotypic interaction with the luminal domain of nesprin-2. Based on previously published in vitro biochemical and structural studies, it is expected that a homotrimer of SUN2 interact with three nesprin-2 KASH peptides to form a heterohexamer (21,22). Moreover, SUN2 homotrimerization was shown to be critical for KASH binding (21,35). To begin to test this model of LINC complex assembly in the NE of living cells, we first performed measurements on cells co-expressing mCherry-SR-KASH2 with SS-EGFP-SUN2$^{595–731}$. The SUN domain (SUN2$^{595–731}$) contains the KASH-binding sites and has previously been shown to remain monomeric using SC tsMSQ (16). Thus, the SUN domain permits us to directly test for the presence of monomer-monomer interactions with nesprin-2.

Fitting the DC tsMSQ curves to Eq. 7 agreed well with the data ($\chi^2_\nu = 0.88$) (Fig. 7 *A*). A plot of b_r versus b_g revealed that the data were clustered around (1, 0), indicating a noninteracting monomeric EGFP-labeled protein species (Fig. 7 *B*). Neither b_g nor b_r showed any concentration dependence, and both have means consistent with SS-EGFP-SUN2$^{595–731}$ being unable to interact with mCherry-SR-KASH2 (Fig. 7 *C*). In addition, the values of τ_D, **A**, and τ_0 all agreed with the expectation of a noninteracting SS-EGFP-SUN2$^{595–731}$ monomer (Figs. S5 *C*, S6 *C*, and S7 *E*). Taken together, these results support the model in which the luminal domain of nesprin-2 is unable to interact with monomers of the SUN2 luminal domain.

Unlike SS-EGFP-SUN2$^{595–731}$, the SUN2 luminal domain-encoding SS-EGFP-SUN2$^{261–731}$ homotrimerizes in the NE of living cells as determined by SC FFS (18). Thus, we expected that measurements performed in the NE of cells co-expressing SS-EGFP-SUN2$^{261–731}$ and mCherry-SR-KASH2 would identify heterotypic interactions between these constructs. Proper analysis by DC tsMSQ of data obtained in cells expressing both proteins required the inclusion of two diffusing species (Eq. 8) to describe the data (Fig. 8 *A*). The two diffusion times have means of 1.7 and 180 ms (Fig. S7 *F*), which are consistent with a previous SC FFS study of SS-EGFP-SUN2$^{261–731}$ (18).The tsMSQ$_{gr}$ amplitude is significantly higher than the noninteracting prediction (Fig. 8 *A*), indicating the presence of heteroprotein association. Plotting b_r versus b_g from $n = 53$ cells revealed that both b_g and b_r increase together (Fig. 8 *B*), implying that an increase in the average oligomeric state of SS-EGFP-SUN2$^{261–731}$ is associated with an

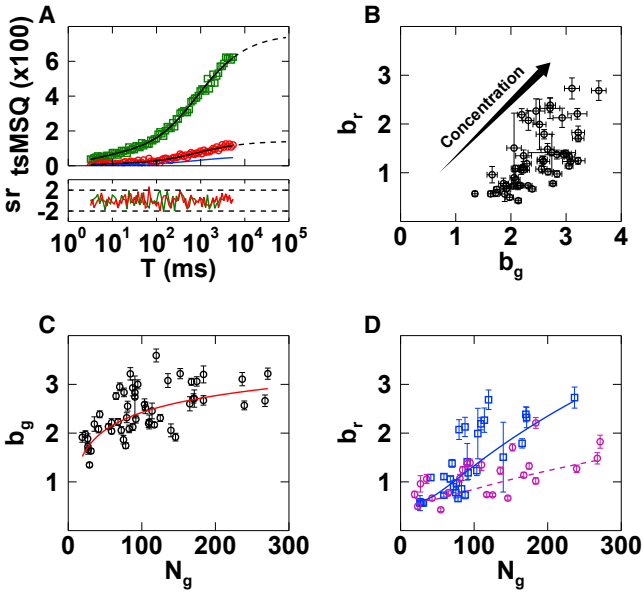

FIGURE 8 DC tsMSQ analysis of measurements performed in the NE of cells ($n = 53$) co-expressing SS-EGFP-SUN2$^{261–731}$ and mCherry-SR-KASH2. (*A*) Shown are tsMSQ curves (*symbols*) with fits (*black lines*) and associated standard residuals (sr) with $\chi^2_r = 0.88$ and predicted $tsMSQ_{gr}^{(-)}$ curve (*blue line*). The $tsMSQ_{gg}$ and $tsMSQ_{gr}$ curves are shown with green squares and red circles, respectively. (*B*) b_r versus b_g with standard deviations (error bars) are correlated and increase with concentration as indicated. (*C*) Shown is b_g versus N_g with standard deviations (error bars) and a line provided to guide the eye. (*D*) Shown is b_r versus N_g with standard deviations (error bars) separated by N_r/N_g ratios greater (*blue squares*) or less (*magenta circles*) than 4:1, with lines provided to guide the eye. To see this figure in color, go online.

increase in the number of bound mCherry-SR-KASH2. This result supports the model that nesprin-2 interacts with homotrimers of SUN2 within the NE. We further notice that $b_r \leq b_g$, indicating that at most, one mCherry-SR-KASH2 can associate with each SS-EGFP-SUN2$^{261–731}$ protein within the homotrimer.

These data show that b_g ranges between 1 and 3, signifying a limiting homotrimeric state for the SS-EGFP-SUN2$^{261–731}$ in the NE. The concentration dependence of the oligomerization of SS-EGFP-SUN2$^{261–731}$ is visualized by a plot of b_g versus N_g (Fig. 8 *C*). The brightness increases with N_g, approaching a homotrimeric brightness state, which is identical to the behavior observed for SS-EGFP-SUN2$^{261–731}$ in the absence of mCherry-SR-KASH2 (16). We expect to observe an increase in b_r with N_g because the luminal domain of nesprin-2 is predicted to bind to homotrimers of the SUN2 luminal domain, which are populated at a higher N_g (Fig. 8 *C*). However, the amount of bound mCherry-SR-KASH2 also depends on its concentration, which varies significantly from cell to cell. Thus, the variability in the expression ratio of mCherry-SR-KASH2 to SS-EGFP-SUN2$^{261–731}$ is responsible for the large scatter in the observed b_r values (Fig. 8 *D*). To visualize the dependence of b_r on the expression ratio of these two constructs, the data were separated into sets with an N_r/N_g above and below 4:1 (Fig. 8 *D*). Data with a N_r/N_g ratio above 4:1 exhibit a strong increase in b_r up to values approaching 3, whereas the lower ratio data only show a modest increase in b_r with N_g. This reflects the relative reduction in mCherry-SR-KASH2 concentration between both data sets. Notably, the highest brightness values measured for b_g and b_r approach 3 (Fig. 8, *B–D*), which suggests the formation of a SUN2-nesprin-2 heterohexamer in vivo as predicted by in vitro models (21,22).

CONCLUSIONS

Although CCF analysis has been widely used to identify heterotypic protein interactions from FFS measurements performed in cells (36), the presence of nuclear membrane undulations is a significant barrier for its application to FFS measurements performed in the NE. The local volume changes caused by nuclear membrane undulations lead to coupled changes in the emission intensity of both the red and green fluorescent labels (Fig. 1 *B*), which result in a spurious cross correlation in the CCF, even when accounting for spectral cross talk. The DC tsMSQ theory developed in this article provides a comprehensive method that incorporates both spectral cross talk and volume fluctuations, thus overcoming the issues present in CCF analysis of FFS data measured in the NE. Although this article has focused on the use of tsMSQ to account for the presence of volume fluctuations, the advantages of tsMSQ extend to any slow fluctuation process. Bias introduced by slow fluctuations is a general challenge for FFS analysis, and tsMSQ provides the ability to identify and account for the effect of these slow processes (14,18). Once a slow fluctuation process has been detected, new models incorporating the process can be developed to account for its effect on the tsMSQ curve. For example, the original formulation of MSQ analysis was used to account for the presence of photodepletion (17).

We experimentally verified DC tsMSQ using model systems representing noninteracting protein pairs as well as heterodimeric protein complexes and recovered diffusion times and HSP brightness values. The label stoichiometry determined by HSP brightness matched the expected values of the control samples and reliably distinguished interacting from noninteracting proteins. Furthermore, the parameters of the volume fluctuation process agreed with our previously published SC tsMSQ results (14), thus providing additional support for the DC tsMSQ model.

Next, we used DC tsMSQ to investigate the assembly mechanism of LINC complexes, which are formed by the heterotypic interaction of the luminal domains of SUN and KASH proteins (37). Previously published in vitro biochemical and structural studies revealed that a homotrimer of the SUN2 luminal domain interacts with three nesprin-2 luminal domains (21,22). Deep KASH peptide-

binding grooves are formed at the interface of two adjacent SUN domains upon SUN2 luminal domain homotrimerization; therefore, SUN2 homotrimerization is believed to be a necessary precursor to the assembly of a SUN2-nesprin-2 heterohexamer (21,22).

To test this model in vivo, we looked for interactions between the luminal domain of nesprin-2 (mCherry-SR-KASH2) and two SS-EGFP-tagged SUN2 luminal domain constructs. We previously showed that the EGFP-tagged luminal domain of SUN2 (SS-EGFP-SUN2$^{261–731}$) forms homotrimers in the NE, whereas the SUN domain of SUN2 (SS-EGFP-SUN2$^{595–731}$) remains monomeric (16). As expected, we were unable to detect a heterotypic interaction between SS-EGFP-SUN2$^{595–731}$ and mCherry-SR-KASH2 using DC tsMSQ. However, DC tsMSQ did detect a concentration-dependent heterotypic interaction between SS-EGFP-SUN2$^{261–731}$ and mCherry-SR-KASH2 in the NE. The limiting HSP brightness values measured for these constructs suggest the formation of a SUN2-nesprin-2 heterohexamer in vivo, which agrees with the in vitro results described above (38).

These initial results provide a promising starting point for future quantitative studies of the mechanisms underlying the in vivo assembly of functional LINC complexes and their regulation. Combining quantitative modeling of the DC tsMSQ brightness data with targeted mutations that perturb the known SUN2-nesprin-1/2 binding sites should provide a comprehensive approach for investigating the assembly of SUN2-containing LINC complexes. In addition, DC tsMSQ offers a tool to investigate the formation of LINC complexes composed of lesser studied SUN proteins, such as SUN1, which forms higher-order oligomers than SUN2 (16). This article focused on luminal domains of SUN2 and nesprin-2 due to the low mobility of the full-length proteins, which prevents us from performing point FFS measurements (39,40). Future work combining DC tsMSQ with an imaging- or scanning-based approach may allow for measurements of LINC complex assembly with full-length proteins. In addition, by combining scanning with the data segmentation inherent to tsMSQ, techniques such as intensity-sorted FCS may be incorporated (41) to look at the assembly of full-length SUN2 and nesprin-2 and investigate the presence of spatial heterogeneity in the assembly process. Although this article has focused on the application of DC tsMSQ for characterizing the heterotypic interactions of LINC complex proteins, the development of DC tsMSQ offers a promising and general platform for future studies of heteroprotein complex formation in the NE of living cells.

SUPPORTING MATERIAL

Supporting Material can be found online at https://doi.org/10.1016/j.bpj.2019.11.020.

AUTHOR CONTRIBUTIONS

J.H., G.W.G.L., and J.D.M. were responsible for experimental design. J.H. performed experiments. K.-H.H. developed analytical tools. J.H., K.-H.H., J.K., S.R.K., I.A., and J.D.M. performed analysis. J.H., K.-H.H., G.W.G.L., and J.D.M. wrote the manuscript.

ACKNOWLEDGMENTS

We thank Cosmo A. Saunders for his help generating the DNA constructs used in this study.

This work was supported by the National Institutes of Health GM064589 (J.D.M, J.H., K.-H.H., J.K., S.R.K., and I.A.) and GM129374 (G.W.G.L., J.D.M., and K.-H.H.).

REFERENCES

1. Jameson, D. M., J. A. Ross, and J. P. Albanesi. 2009. Fluorescence fluctuation spectroscopy: ushering in a new age of enlightenment for cellular dynamics. *Biophys. Rev.* 1:105–118.
2. Petersen, N. O., P. L. Höddelius, …, K. E. Magnusson. 1993. Quantitation of membrane receptor distributions by image correlation spectroscopy: concept and application. *Biophys. J.* 65:1135–1146.
3. Chen, Y., J. D. Müller, …, E. Gratton. 1999. The photon counting histogram in fluorescence fluctuation spectroscopy. *Biophys. J.* 77:553–567.
4. Müller, J. D. 2004. Cumulant analysis in fluorescence fluctuation spectroscopy. *Biophys. J.* 86:3981–3992.
5. Digman, M. A., R. Dalal, …, E. Gratton. 2008. Mapping the number of molecules and brightness in the laser scanning microscope. *Biophys. J.* 94:2320–2332.
6. Schwille, P., F. J. Meyer-Almes, and R. Rigler. 1997. Dual-color fluorescence cross-correlation spectroscopy for multicomponent diffusional analysis in solution. *Biophys. J.* 72:1878–1886.
7. Wu, B., Y. Chen, and J. D. Müller. 2010. Heterospecies partition analysis reveals binding curve and stoichiometry of protein interactions in living cells. *Proc. Natl. Acad. Sci. USA.* 107:4117–4122.
8. Chen, Y., M. Tekmen, …, J. D. Müller. 2005. Dual-color photon-counting histogram. *Biophys. J.* 88:2177–2192.
9. Chen, Y., L. N. Wei, and J. D. Müller. 2003. Probing protein oligomerization in living cells with fluorescence fluctuation spectroscopy. *Proc. Natl. Acad. Sci. USA.* 100:15492–15497.
10. Wiedenmann, J., F. Oswald, and G. U. Nienhaus. 2009. Fluorescent proteins for live cell imaging: opportunities, limitations, and challenges. *IUBMB Life.* 61:1029–1042.
11. Chen, Y., L. N. Wei, and J. D. Müller. 2005. Unraveling protein-protein interactions in living cells with fluorescence fluctuation brightness analysis. *Biophys. J.* 88:4366–4377.
12. Macdonald, P. J., Y. Chen, …, J. D. Mueller. 2010. Brightness analysis by Z-scan fluorescence fluctuation spectroscopy for the study of protein interactions within living cells. *Biophys. J.* 99:979–988.
13. Smith, E. M., P. J. Macdonald, …, J. D. Mueller. 2014. Quantifying protein-protein interactions of peripheral membrane proteins by fluorescence brightness analysis. *Biophys. J.* 107:66–75.
14. Hennen, J., K. H. Hur, …, J. D. Mueller. 2017. Quantitative brightness analysis of protein oligomerization in the nuclear envelope. *Biophys. J.* 113:138–147.
15. Dauer, W. T., and H. J. Worman. 2009. The nuclear envelope as a signaling node in development and disease. *Dev. Cell.* 17:626–638.
16. Hennen, J., C. A. Saunders, …, G. W. G. Luxton. 2018. Fluorescence fluctuation spectroscopy reveals differential SUN protein oligomerization in living cells. *Mol. Biol. Cell.* 29:1003–1011.
17. Hur, K. H., and J. D. Mueller. 2015. Quantitative brightness analysis of fluorescence intensity fluctuations in E. Coli. *PLoS One.* 10:e0130063.

18. Hennen, J., K. H. Hur, …, J. D. Mueller. 2019. Protein oligomerization and mobility within the nuclear envelope evaluated by the time-shifted mean-segmented Q factor. *Methods.* 157:28–41.
19. Meinke, P., and E. C. Schirmer. 2015. LINC'ing form and function at the nuclear envelope. *FEBS Lett.* 589:2514–2521.
20. Lombardi, M. L., D. E. Jaalouk, …, J. Lammerding. 2011. The interaction between nesprins and sun proteins at the nuclear envelope is critical for force transmission between the nucleus and cytoskeleton. *J. Biol. Chem.* 286:26743–26753.
21. Sosa, B. A., A. Rothballer, …, T. U. Schwartz. 2012. LINC complexes form by binding of three KASH peptides to domain interfaces of trimeric SUN proteins. *Cell.* 149:1035–1047.
22. Wang, W., Z. Shi, …, Z. Zhou. 2012. Structural insights into SUN-KASH complexes across the nuclear envelope. *Cell Res.* 22:1440–1452.
23. Sanchez-Andres, A., Y. Chen, and J. D. Müller. 2005. Molecular brightness determined from a generalized form of Mandel's Q-parameter. *Biophys. J.* 89:3531–3547.
24. Hennen, J., I. Angert, …, J. D. Mueller. 2018. Investigating LINC complex protein homo-oligomerization in the nuclear envelopes of living cells using fluorescence fluctuation spectroscopy. *Methods Mol. Biol.* 1840:121–135.
25. Smith, E. M., J. Hennen, …, J. D. Mueller. 2015. Z-scan fluorescence profile deconvolution of cytosolic and membrane-associated protein populations. *Anal. Biochem.* 480:11–20.
26. Hur, K. H., Y. Chen, and J. D. Mueller. 2016. Characterization of ternary protein systems in vivo with tricolor heterospecies partition analysis. *Biophys. J.* 110:1158–1167.
27. Wu, B., Y. Chen, and J. D. Müller. 2009. Fluorescence fluctuation spectroscopy of mCherry in living cells. *Biophys. J.* 96:2391–2404.
28. Wu, B., and J. D. Müller. 2005. Time-integrated fluorescence cumulant analysis in fluorescence fluctuation spectroscopy. *Biophys. J.* 89:2721–2735.
29. Chen, Y., and J. D. Müller. 2007. Determining the stoichiometry of protein heterocomplexes in living cells with fluorescence fluctuation spectroscopy. *Proc. Natl. Acad. Sci. USA.* 104:3147–3152.
30. Liu, Z., A. Zolkiewska, and M. Zolkiewski. 2003. Characterization of human torsinA and its dystonia-associated mutant form. *Biochem. J.* 374:117–122.
31. Bacia, K., and P. Schwille. 2007. Practical guidelines for dual-color fluorescence cross-correlation spectroscopy. *Nat. Protoc.* 2:2842–2856.
32. Patterson, G., R. N. Day, and D. Piston. 2001. Fluorescent protein spectra. *J. Cell Sci.* 114:837–838.
33. Chen, Y., J. D. Müller, …, E. Gratton. 2002. Molecular brightness characterization of EGFP in vivo by fluorescence fluctuation spectroscopy. *Biophys. J.* 82:133–144.
34. Vander Heyden, A. B., T. V. Naismith, …, P. I. Hanson. 2011. Static retention of the lumenal monotopic membrane protein torsinA in the endoplasmic reticulum. *EMBO J.* 30:3217–3231.
35. Nie, S., H. Ke, …, W. Feng. 2016. Coiled-coil domains of SUN proteins as intrinsic dynamic regulators. *Structure.* 24:80–91.
36. Bacia, K., I. V. Majoul, and P. Schwille. 2002. Probing the endocytic pathway in live cells using dual-color fluorescence cross-correlation analysis. *Biophys. J.* 83:1184–1193.
37. Crisp, M., Q. Liu, …, D. Hodzic. 2006. Coupling of the nucleus and cytoplasm: role of the LINC complex. *J. Cell Biol.* 172:41–53.
38. Sosa, B. A., U. Kutay, and T. U. Schwartz. 2013. Structural insights into LINC complexes. *Curr. Opin. Struct. Biol.* 23:285–291.
39. Ostlund, C., E. S. Folker, …, H. J. Worman. 2009. Dynamics and molecular interactions of linker of nucleoskeleton and cytoskeleton (LINC) complex proteins. *J. Cell Sci.* 122:4099–4108.
40. Hur, K. H., P. J. Macdonald, …, J. D. Mueller. 2014. Quantitative measurement of brightness from living cells in the presence of photodepletion. *PLoS One.* 9:e97440.
41. Di Bona, M., M. A. Mancini, …, L. Lanzanò. 2019. Measuring mobility in chromatin by intensity-sorted FCS. *Biophys. J.* 116:987–999.